19th WORLD CONFERENCE OF THE ASSOCIATED RESEARCH CENTRES FOR THE URBAN UNDERGROUND SPACE
Belgrade, Serbia, November 4-7, 2025.

ACUUS BELGRADE 2025

Paper No: 4.12.94
DOI: 10.46793/ACUUS2025.4.12.94

INFLUENCE OF GEOMETRIC PARAMETERS AND VELOCITY OF VENT ON HEAVY GAS EXHAUST EFFICIENCY IN TUNNELS

Yuanqing Ma[1], Tianqi Wang[2], Ying Zhang[3], Angui Li[4]

Abstract: Underground spaces are relatively enclosed, which imposes stringent requirements on ensuring personnel safety and achieving effective removal of harmful gases. Notably, high-density harmful gases (hereafter referred to as "heavy gases") tend to accumulate in human breathing zones, posing a severe threat of fatalities and injuries. Consequently, research on exhaust strategies to enhance the removal efficiency of heavy gases in tunnels has become an urgent necessity. In this study, a series of computational fluid dynamics (CFD) simulations were conducted to investigate the removal process of heavy gas contaminants in tunnels. Specifically, the effects of three key parameters—namely the aspect ratio (w/h), vent area (A), and vent height (h_f)—on the performance of side-mounted exhaust vents for addressing heavy gas leakage in tunnels were systematically analyzed. The results reveal that with the increase in w/h and A, both the height of the heavy gas layer downstream of the vent and the heavy gas density exhibit a decreasing trend. However, excessively large A and h_f can lead to the discharge of fresh air through the vents when the exhaust velocity is low, which is detrimental to the overall exhaust efficiency. Within the parameter range investigated in this study, an optimal vent height of 0.1 m was identified. Furthermore, the highest exhaust efficiency of 0.18 was achieved when the vent area was 2 m^2 and the exhaust velocity was 6 m/s. The findings of this research provide a theoretical and data-driven basis for the optimal design of ventilation systems tailored to heavy gas control, thereby facilitating the effective removal of heavy gases in underground spaces.

Keywords: Heavy gas; Underground Space; Side exhaust; Exhaust efficiency; Gas leakage.

1. INTRODUCTION

Due to the development demands of advanced industrial manufacturing and carbon transportation, higher requirements are imposed on the utilization, transportation, and storage of specialty gases (Zeng et al., 2021). Most specialty gases exhibit higher density than air, and once their concentration exceeds a specific threshold, they turn toxic and pose severe hazards to human health (Cai et al., 2020). Under the influence of the negative buoyancy effect, such heavy gases tend to accumulate and spread in the lower regions of enclosed spaces (e.g., industrial workshops, storage warehouses) (Ma et al., 2023). In recent years, improper storage and usage practices have frequently triggered heavy gas leakage accidents, leading to significant casualties and massive economic losses (Hou et al., 2021). Consequently, conducting research on the leakage mechanisms and exhaust characteristics of heavy gases carries substantial theoretical significance. It provides critical support for optimizing personnel evacuation designs, enhancing hazard prediction systems, and developing high-efficiency ventilation systems (Wang et al., 2024). Therefore, investigating the laws governing heavy gas leakage and elimination is of profound theoretical value for improving safety management in related fields.

[1] PhD student, Ma Yuanqing, Heating, Gas Supply, Ventilating and Air Conditioning Engineering, School of Building Services Science and Engineering, Xi'an University of Architecture and Technology, 710055 Xi'an, China, myq_c@xauat.edu.cn.
[2] PhD student, Wang Tianqi, Heating, Gas Supply, Ventilating and Air Conditioning Engineering, School of Building Services Science and Engineering, Xi'an University of Architecture and Technology, 710055 Xi'an,
[3] Dr., Zhang Ying, Heating, Gas Supply, Ventilating and Air Conditioning Engineering, School of Building Services Science and Engineering, Xi'an University of Architecture and Technology, 710055 Xi'an, China, myq_c@xauat.edu.cn.
[4] Professor, Li Angui, Heating, Gas Supply, Ventilating and Air Conditioning Engineering, School of Building Services Science and Engineering, Xi'an University of Architecture and Technology, 710055 Xi'an, liangui@xauat.edu.cn

Extensive research has been conducted on the leakage and diffusion characteristics of heavy gases. However, the majority of existing studies focus primarily on leakage scenarios in industrial workshops (Kassomenos et al., 2008) and open atmospheric environments (Blackmore et al., 1982; Hanna et al., 1993). For instance, Li et al. (Li et al., 2023b) employed numerical simulations to investigate how the diameter and shape of leakage sources affect the diffusion characteristics of R290 in an enclosed room following leakage, while further analyzing the explosion risks induced by R290 leakage. Wang et al. (Wang et al., 2013) used computational fluid dynamics (CFD) to study the continuous release and diffusion process of carbon dioxide (CO_2) in a ventilated industrial workshop, and analyzed the effects of release rate, airflow velocity, and obstacles on CO_2 propagation. Gao et al. (Gao et al., 2023) examined the concentration distribution of heavy gases with different densities and the effectiveness of integrated ventilation systems in a typical office space. Li et al. (Li et al., 2023a) simulated the impact of the speed and size of moving obstacles in a chemical plant on chlorine (Cl_2) leakage diffusion. Additionally, Fatahian et al. (Fatahian et al., 2020) demonstrated via CFD simulations that the gas mass fraction increases significantly immediately after release. Notably, there remains a paucity of research on heavy gas leakage and diffusion accidents in narrow and long spaces (e.g., tunnels). In particular, the relationship between the emission behavior of hazardous gases and ventilation system performance in such narrow and long spaces has not been clearly elucidated.

Research on ventilation systems specifically tailored to heavy gas control also remains limited. Currently, most ventilation facilities in tunnels are installed at the top of the space, primarily designed for removing flue gases (a type of positively buoyant gas)(Cong et al., 2021; Lei et al., 2023). In contrast, vent positions for scenarios involving potential heavy gas leakage are mostly determined based on empirical experience. This empirical approach not only fails to fully exploit the performance potential of ventilation equipment but also leads to unnecessary resource waste.

Prior studies have suggested that vents should be installed on the lower sides of enclosed spaces; this configuration allows heavy gases to be exhausted via a shorter path, thereby minimizing the scope of their hazardous impact (Han et al., 2020). However, further research is still required to optimize the design parameters (e.g., vent size, airflow rate) and spatial positions of such heavy gas-targeted ventilation systems (Wang et al., 2025).

Against this backdrop, this study designed a total of 55 simulation cases to investigate the heavy gas elimination performance of side-mounted vents in a tunnel. Specifically, the extraction efficiency of vents with different aspect ratios, cross-sectional areas, and heights above the ground was compared. Within the parameter range investigated in this study, the optimal parameters and spatial positions of side-mounted vents for heavy gas elimination were analyzed. The findings of this research provide a theoretical and technical basis for the optimal design of exhaust systems addressing heavy gas leakage in underground spaces (e.g., tunnels).

2. NUMERICAL SIMULATION METHOD

2.1. Governing equations

The spatial dispersion behavior of heavy gas flows can be efficiently analyzed using the professional computational fluid dynamics (CFD) software FLUENT (Zhang et al., 2020). Turbulent flow effects in such scenarios can be modeled via three primary approaches: the Reynolds-Averaged Navier – Stokes (RANS) method, Large Eddy Simulation (LES), or fully resolved through Direct Numerical Simulation (DNS). A review of existing literature on heavy gas turbulent flow simulation reveals that the RANS method offers an optimal balance between result accuracy and computational efficiency—this compromise makes it well-suited for engineering-scale studies. Given that the primary objective of this research is to analyze the steady-state elimination of heavy gases, the Reynolds time-averaged Navier – Stokes (RANS) equations were selected as the governing equations. All simulations in this study were implemented using FLUENT, where the Navier – Stokes equations were solved by coupling the fundamental equations of continuity, momentum, and species transport. The core governing equations are presented as follows (Inc, 2022):

$$\frac{\partial \rho}{\partial t} + div(\rho u_i) = 0 \tag{1}$$

$$\frac{\partial u_i}{\partial t} + (u_i \cdot \nabla) u_i = -\frac{1}{\rho}\nabla p + \frac{\mu}{\rho}\Delta u_i + F_{bi} \tag{2}$$

$$\frac{\partial c}{\partial t} + u_j \frac{\partial c}{\partial x_i} = \frac{\partial}{\partial x_j}(D\frac{\partial c}{\partial x_j}) \tag{3}$$

where μ is the dynamic viscosity, mPa·s; ρ is the density of the mixture, kg/m^3; F_{bi} is the mass force, N/kg; c is the concentration of heavy gas; D is the diffusion coefficient of heavy gas.

Table 1. *Details of CFD boundary conditions.*

Parameter	Value
Cases	Steady, 3-D calculations
Fluid	SF_6
Far field	Pressure outlet: 0-gauge pressure
Inlet	Velocity: 10 ~ 15 m/s Hydraulic diameter = 0.5 m
Vent	Velocity: 6 ~ 14 m/s
Ground	Wall (no slip)

2.2. Geometric model

A typical tunnel was selected as the research object, and the geometric dimensions of the computational domain are illustrated in Figure 1. The heavy gas leakage source was positioned at the center of the tunnel bottom, with a diameter of 0.5 m. Four symmetrically arranged side vents were installed on both sides of the tunnel; their specific geometric dimensions and spatial positions are provided in Figure 1. Sulfur hexafluoride (SF_6) was chosen as the surrogate for heavy gas in the leakage simulations, and a velocity inlet boundary condition was applied to the leakage source to simulate continuous gas release. All vents were set as velocity outlets, with the exhaust velocity (u_e) varied at five levels: 6, 8, 10, 12, and 14 m/s. Additionally, pressure outlet boundary conditions were assigned to both ends of the tunnel, while the tunnel walls were set to a no-slip boundary condition. Detailed specifications of the CFD boundary conditions are summarized in Table 1.

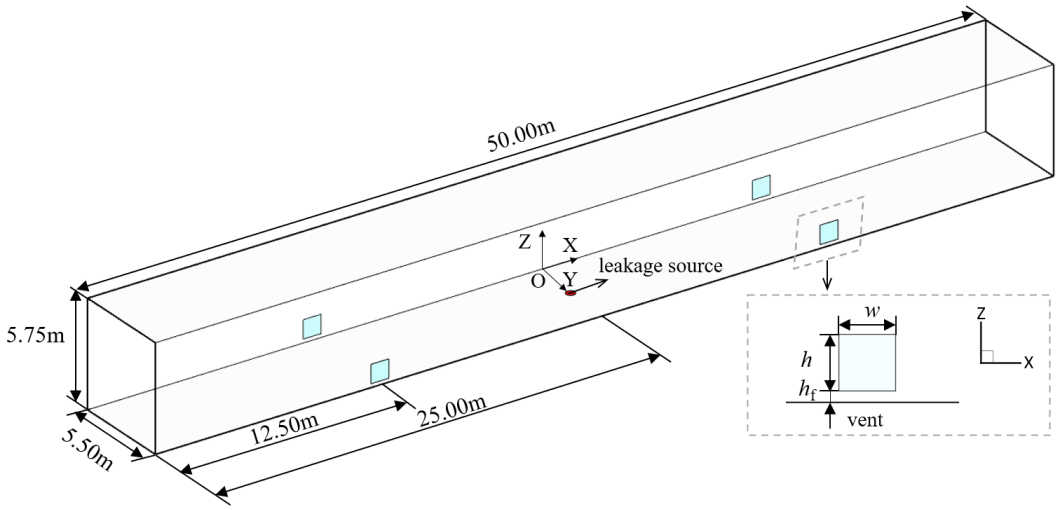

Figure 1. *Schematic of the computational domain*

In this study, four sets of key parameters were designed to investigate their effects on heavy gas elimination performance, with the following variable levels:

Vent area (A) : 1.00, 1.30, 1.54, and 2.00 m^2 ;

Vent aspect ratio (w/h): 1.00, 1.30, 1.53, and 2.00;

Vent height above the ground (h_f): 0.10, 0.20, 0.30, and 0.50 m;

Exhaust velocity (u_e): 6, 8, 10, 12, and 14 m/s.

A total of 55 experimental conditions were designed in this study, with detailed parameter combinations provided in Table 2. Among these, Cases 53~55 were conducted under the condition of non-functional vents (i.e., vents not in operation). The primary purpose of these three cases was to measure the height of the heavy gas layer h_t under different leakage intensities, providing a baseline reference for analyzing the effect of vent operation on heavy gas elimination.

Table 2. *Simulation conditions.*

Case	w (m)	w/h	$w \times h$ (m^2)	h_f (m)	Q_0 (m^3/s)	u_e (m/s)
1					1.96	8.00.
2					2.36	8.00
3	1.00	1.00	1.00	0.20	2.94	8.00
4					2.36	6.00
5					2.36	10.00

6					2.36	12.00
7					2.36	14.00
8						6.00
9						8.00
10				0.10	2.36	10.00
11						12.00
12						14.00
13						6.00
14						8.00
15				0.30	2.36	10.00
16						12.00
17						14.00
18						6.00
19						8.00
20				0.50	2.36	10.00
21						12.00
22						14.00
23						6.00
24						8.00
25	1.14	1.30	1.00	0.20	2.36	10.00
26						12.00
27						14.00
28						6.00
29						8.00
30	1.24	1.53	1.00	0.20	2.36	10.00
31						12.00
32						14.00
33						6.00
34						8.00
35	1.41	2.00	1.00	0.20	2.36	10.00
36						12.00
37						14.00
38						6.00
39						8.00
40	1.14	1.00	1.30	0.20	2.36	10.00
41						12.00
42						14.00
43						6.00
44						8.00
45	1.24	1.00	1.54	0.20	2.36	10.00
46						12.00
47						14.00
48						6.00
49						8.00
50	1.41	1.00	2.00	0.20	2.36	10.00
51						12.00
52						14.00
53					1.96	\
54	1.00	1.00	1.00	1.00	2.36	\
55					2.94	\

The volume flux of the inlet Q_0 can be expressed as：

$$Q_0 = \pi \frac{D^2}{4} u_0 \tag{4}$$

where D is the diameter of the leakage source, m; u_0 is the velocity of the leakage source, m/s.

2.3. Grid independence verification and turbulence model validation

Prior studies have indicated that grid resolution is a key factor influencing the prediction accuracy and computational cost-effectiveness of buoyancy-driven flow simulations (Ma et al., 2025). To investigate the impact of grid resolution on simulation results, four structured hexahedral grid systems with different cell counts were

constructed prior to the formal CFD simulations: Grid System A (970,425 cells), Grid System B (1,262,029 cells), Grid System C (1,592,045 cells), and Grid System D (1,982,439 cells). Given the high density gradients and velocity gradients near the leakage inlet (where flow field changes are most significant), local mesh refinement was implemented in this region to capture the detailed flow characteristics. The overall mesh structure of Grid System C and a magnified view of the refined mesh near the leakage inlet are presented in Figure 2.

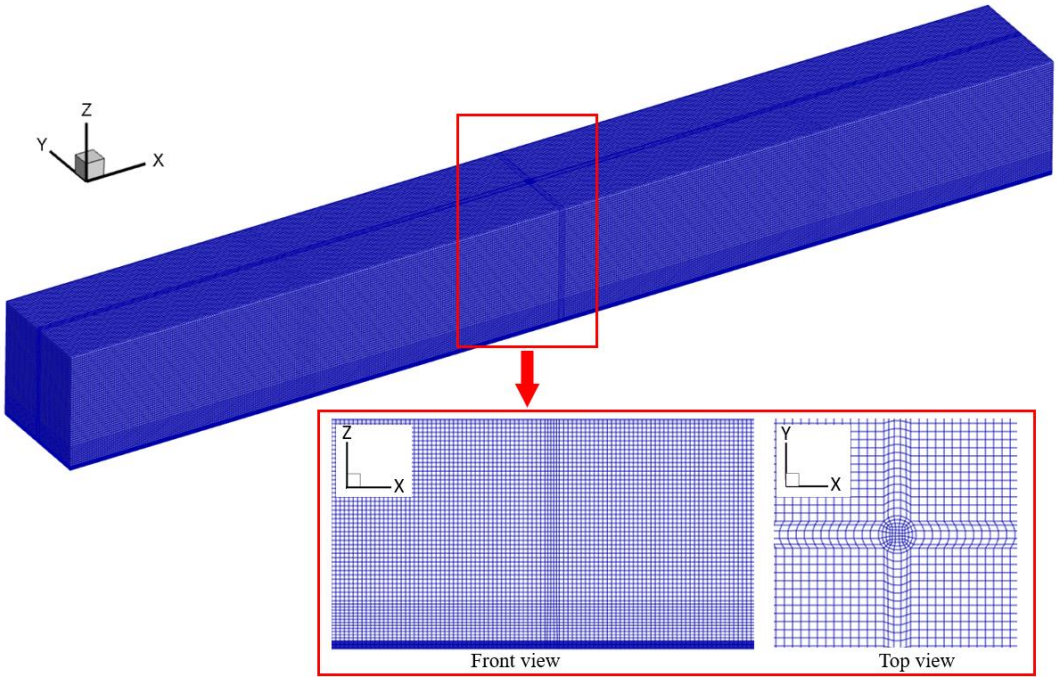

Figure 2. *Details of grid system C*

Figure 3 presents the density and velocity profiles along the centerline at Z = 0.7 m for the four grid systems. It can be observed that the simulation results of Grid System C and Grid System D are relatively consistent, indicating that the solution tends to converge when the grid density reaches the level of Grid System C.

To further quantify the prediction accuracy of each grid system, three commonly used evaluation metrics were adopted: Mean Absolute Error (MAE), Mean Square Error (MSE), and Mean Absolute Percentage Error (MAPE). The simulation results of the four grid systems were compared with the results obtained from Large Eddy Simulation (LES) (serving as a high-fidelity reference) to calculate the prediction errors for each grid. The detailed error calculation results are summarized in Table 3, where it is shown that the MAPE values of both Grid System C and Grid System D are less than 10%—a threshold generally considered acceptable for engineering simulations.

Considering the balance between computational accuracy and computational cost (Grid System D requires significantly higher computational resources than Grid System C while providing negligible accuracy improvement), Grid System C was ultimately selected as the optimal grid configuration for all subsequent simulations in this study.

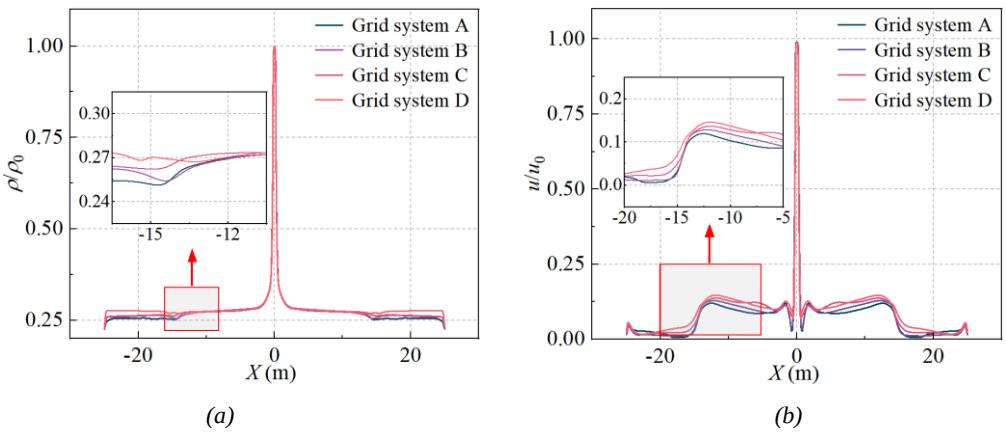

Figure 3. *Density and velocity profiles of four grid systems (a) Density; (b) velocity.*

Table 3. *Detailed parameters of the grid system.*

Grid system	Total number of cells	Error with LES					
		ρ / ρ_0			u / u_0		
		MAE	MSE	MAPE	MAE	MSE	MAPE
A	970,425	0.31	0.81	15.88%	0.10	0.05	23.31%
B	1,262,029	0.29	0.76	14.34%	0.09	0.05	16.40%
C	1,592,045	0.20	0.54	8.26%	0.08	0.04	9.70%
D	1,982,439	0.05	0.05	3.37%	0.03	0.01	5.56%

To identify the most appropriate turbulence model for the present study, five typical turbulence models were selected for verification and comparison: the standard k-ε model, SST k-ω model, realizable k-ε model, RNG k-ε model, and standard k-ω model.

Figure 4 presents a comparison between the simulation results of these five turbulence models and the Large Eddy Simulation (LES) results (used as the high-fidelity reference) regarding the centerline density decay and centerline velocity decay of the vent. Among the models tested, the standard k-ω model exhibited more accurate profile characteristics for the vertical centerline velocity.

Quantitatively, the deviations between the vent centerline density decay predicted by each turbulence model and the LES results are as follows: 12.30% (standard k-ε model), 9.10% (SST k-ω model), 4.66% (realizable k-ε model), 6.67% (RNG k-ε model), and 2.86% (standard k-ω model). Similarly, the deviations in vent centerline velocity decay from the LES results are: 11.04% (standard k-ε model), 14.04% (SST k-ω model), 2.30% (realizable k-ε model), 10.38% (RNG k-ε model), and 2.28% (standard k-ω model).

Combined with the above quantitative and qualitative analysis, as well as consistent findings from previous literature (Xing et al., 2013; Zhang et al., 2020), the standard k-ω model was determined to be suitable for predicting the propagation and elimination processes of heavy gases in this study.

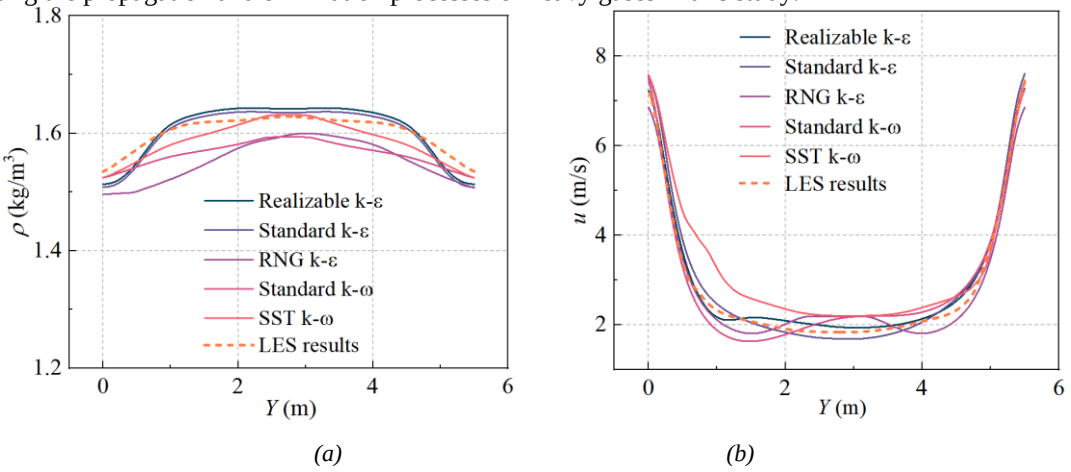

Figure 4. *Density and velocity decay of different turbulence models. (a) Density; (b) velocity.*

3. RESULTS AND DISCUSSIONS

3.1. Heavy gas height of downstream vent

When heavy gas leakage occurs in a tunnel, the contaminant gas exhibits obvious stratification due to the negative buoyancy effect: it tends to accumulate in the lower region of the tunnel and propagate longitudinally along the ground. Once the side vents on both sides of the tunnel are activated, the heavy gas can be rapidly discharged through these side vents via a shorter flow path—this configuration leverages the low-altitude distribution of heavy gas to enhance exhaust efficiency.

As the exhaust velocity increases, the exhaust air volume rises accordingly, which in turn reduces the height of the heavy gas layer (h_e). However, when h_e drops below the upper edge of the side vents, a significant amount of fresh air (from the upper region of the tunnel) is drawn into the vents. This phenomenon dilutes the heavy gas concentration at the vent inlet, ultimately leading to a decline in heavy gas elimination efficiency.

The primary objective of this study is to optimize the design of exhaust systems for high-density gases. From a mechanistic perspective, the key focus is to minimize the occurrence of fresh air entrainment, thereby ensuring

the stable and efficient operation of the exhaust system. The top view and front view of the heavy gas flow pattern under exhaust velocities ranging from 6 m/s to 14 m/s are presented in Figure 5.

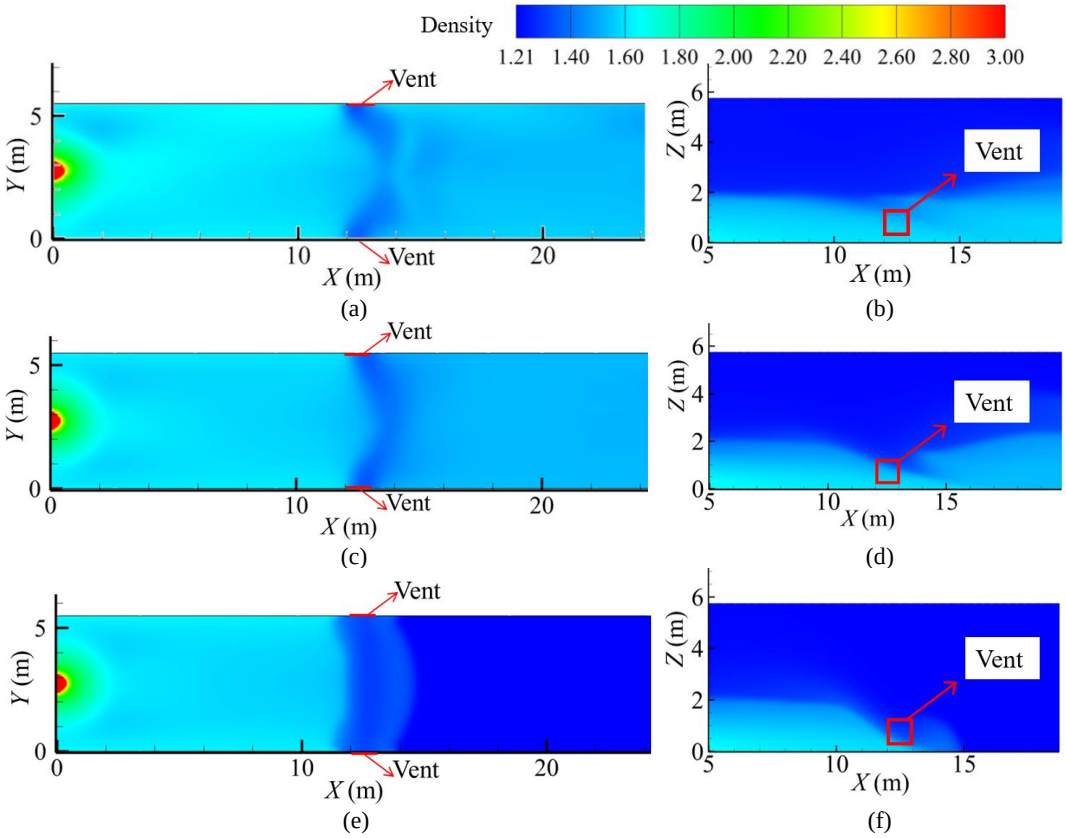

Figure 5. *Heavy gas flow pattern under different exhaust velocities*

(a) ue=6m/s, top view; (b) ue=6m/s, front view; (c) ue=10m/s, top view; (d) ue=10m/s, front view; (e) ue=14m/s, top view; (f) ue=14m/s, front view.

When upper vents (i.e., top-mounted vents) are used, the height of the heavy gas layer is higher compared to the scenario without exhaust. Moreover, upper vents disrupt the stable stratification of heavy gas and expand the scope of heavy gas contamination.

The heavy gas elimination performance is closely associated with the vent layout density (i.e., number of vents per unit tunnel length) and the tunnel's geometric characteristics. As the exhaust velocity increases, the height of the heavy gas layer downstream of the vents (h_e) decreases gradually, as illustrated in the side view of Figure 6.

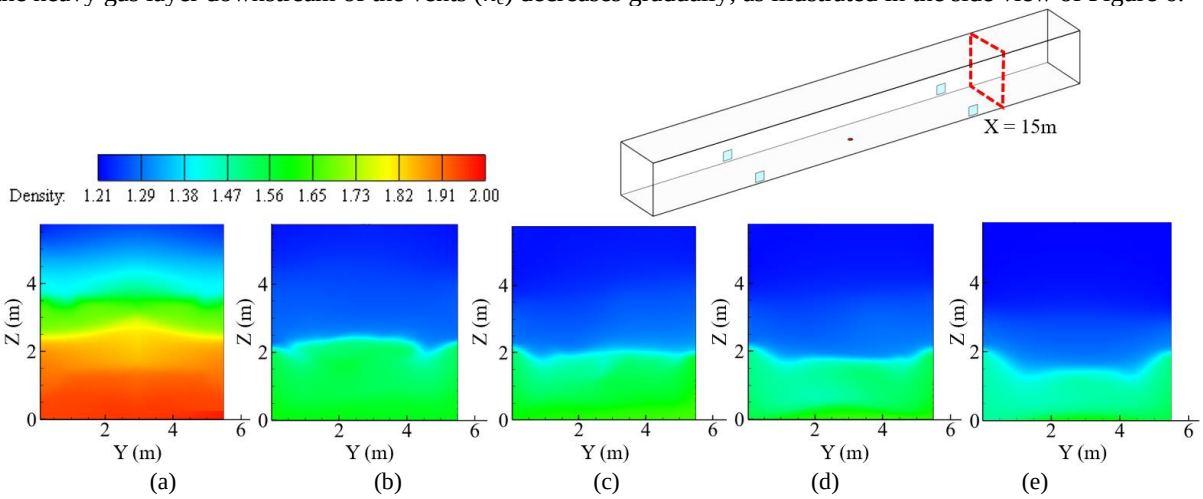

Figure 6. *Heavy gas height at X=15m*

(a) ue=8m/s, top exhaust; (b) ue=6m/s, Case 4; (c) ue=8m/s, Case 5; (d) ue=10m/s, Case 6 ; (e) ue=12m/s, Case 7.

When the inlet volume flux Q_0 of the heavy gas leakage source is 2.36 m^3/s and the exhaust volume of a single side vent exceeds 8 m^3/s (see Figure 7(c)), the height of the heavy gas layer drops below the upper edge of the vent. This triggers the formation of a concave region in the heavy gas layer at the vent location, with the corresponding side view presented in Figure 7.

As the exhaust volume continues to increase, the height of the heavy gas layer downstream of the vent decreases gradually. However, when the exhaust volume further rises (e.g., reaching the level corresponding to Figure 7 (e)), the amount of fresh air entrained into the vent increases significantly. When the exhaust volume increases to 12 m^3/s, the entrainment and discharge of fresh air through the vent become particularly prominent—this phenomenon dilutes the heavy gas concentration at the vent inlet and undermines the overall elimination efficiency.

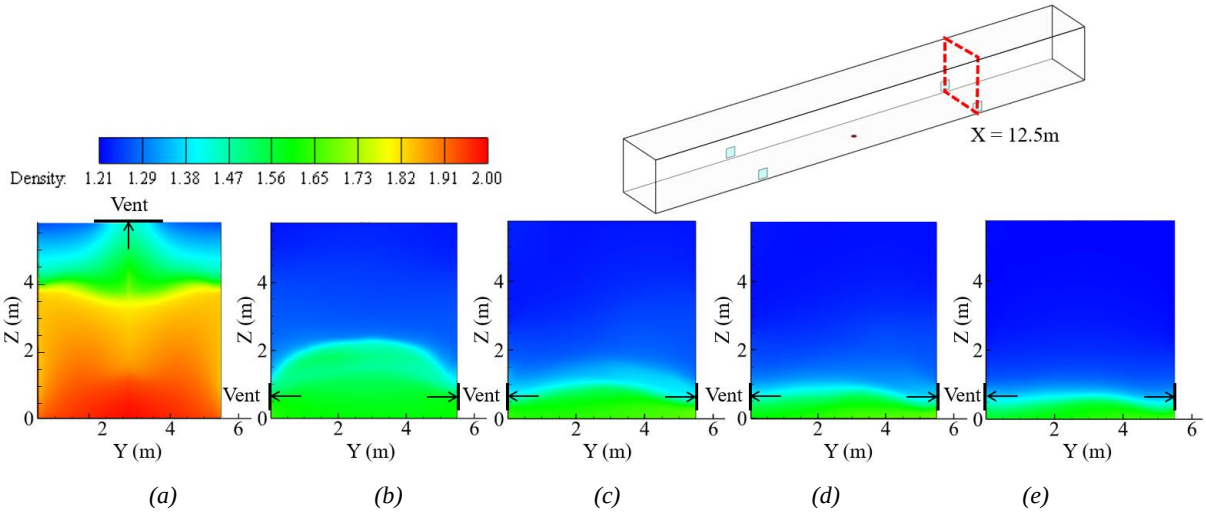

Figure 7. *Heavy gas height at X=12.5m*

(a) ue=8m/s, top exhaust; (b) ue=6m/s, Case 4; (c) ue=8m/s, Case 5; (d) ue=10m/s, Case 6 ; (e) ue=12m/s, Case 7.

The suppression effect of the exhaust system on heavy gas propagation can be quantified using the ratio of the heavy gas layer height downstream of the vent (h_e) to the heavy gas layer height without exhaust (h_t, i.e., the baseline height). As shown in Figure 8, the decreasing trend of the h_e/h_t ratio gradually slows down with the increase in exhaust velocity (u_e). This phenomenon is attributed to the entrainment and discharge of fresh air by the vents, which dilutes the heavy gas concentration at the vent inlet and thereby reduces the heavy gas elimination efficiency.

Figure 8(a) illustrates the variation of the h_e/h_t ratio with increasing u_e. Within the parameter range of this study, it can be observed that under the same exhaust velocity (u_e), the heavy gas layer height downstream of the vent (h_e) decreases as the vent aspect ratio (w/h) increases. The underlying mechanism is that, for vents with the same cross-sectional area, a higher aspect ratio corresponds to a lower vent height (h_e); this lower height makes it easier for fresh air to be entrained into the vents even at relatively low exhaust velocities (u_e), thereby enhancing the suppression of heavy gas propagation.

Figures 8(b) and 8(c) depict the variation of the h_e/h_t ratio under different vent areas (A) and vent heights above the ground (h_f), respectively. The results indicate that an increase in vent area (A) and a decrease in vent height (h_f) can effectively enhance the suppression effect on heavy gas propagation while maintaining the stability of the heavy gas stratification—this is because larger vent areas and lower vent heights are more conducive to capturing the low-altitude heavy gas layer without excessive fresh air entrainment.

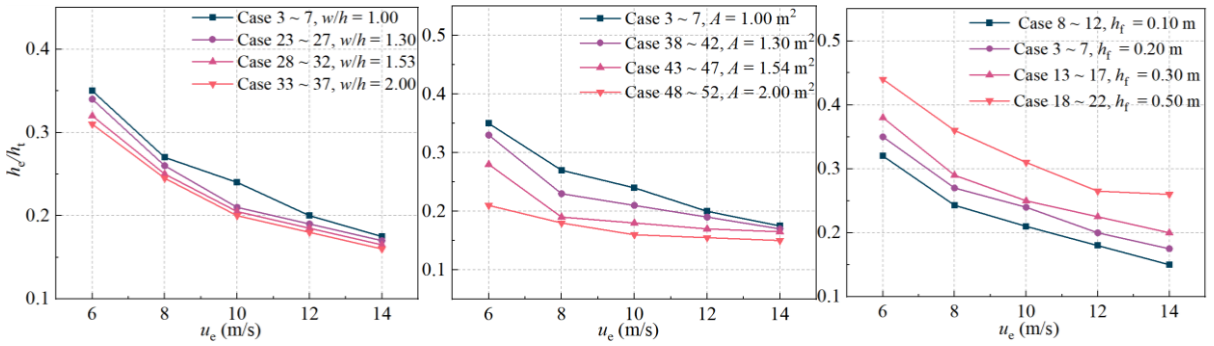

(a) *(b)* *(c)*

Figure 8. *Variation of h_e/h_t under different (a) w/h; (b) vent area; (c) h_f.*

3.2. Average density of vent and Froude number

Since the density difference between heavy gas and air, the mass flow flux of pollutants discharged from the vent can be expressed as:

$$M_e = u_e w \int_{h_f}^{h_t+h} \rho_e dz \tag{5}$$

where u_e is exhaust velocity, m/s; w is the width of the vent, m; h is the height of the vent, m; h_f is the vent height above the floor, m; ρ_e is the density of heavy gas exhaust through the vent, kg/m^3.

The average density of heavy gas discharged from the vent can be expressed as:

$$\rho = \frac{M_e}{u_e w h} \tag{6}$$

A modified Froude number is introduced, which represents the ratio of inertial force to buoyancy. Froude number Fr of exhaust outlet can be expressed as:

$$Fr = \frac{u_e}{Lg(\rho - \rho_a)/\rho_a} \tag{7}$$

Where ρ_a is the ambient density, kg/m^3; L is the characteristic length of tuyere, m; g is the acceleration of gravity, 9.81 kg/m^3.

From Figures 9 (a)~(c), it can be observed that the effect of w/h on ρ is negligible. In contrast, an increase in A exerts a significant influence on ρ, while h only has a certain effect under low exhaust velocities (u_e). Additionally, under the same exhaust volume, a higher average heavy gas density at the vent inlet corresponds to a higher ρ—this is because a denser heavy gas concentration at the vent indicates more effective capture of the target contaminant, rather than excessive entrainment of fresh air.

The Froude number (Fr) is defined as the ratio of inertial force to buoyancy force, which characterizes the relative dominance of these two forces in the flow field. As shown in Figure 9(d), increasing A significantly increases the Fr value at the vent. A higher Fr indicates that inertial force becomes more dominant than buoyancy force in the exhaust flow, meaning the momentum consumed for heavy gas elimination is greater—this further explains why a larger vent area enhances the ability to overcome the negative buoyancy of heavy gas and improve elimination efficiency.

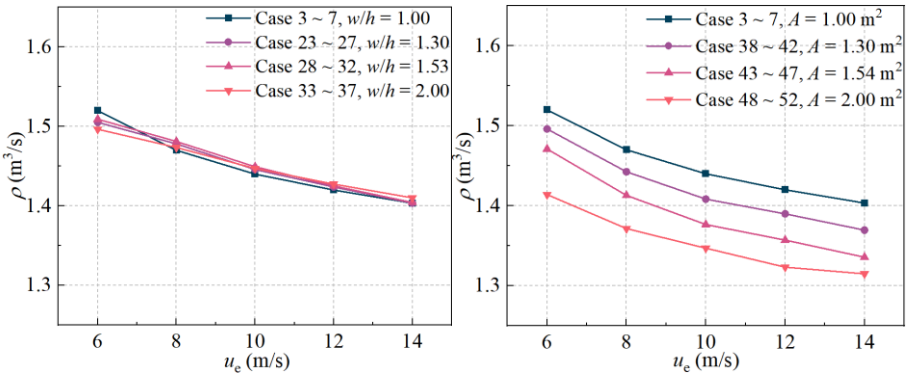

(a) *(b)*

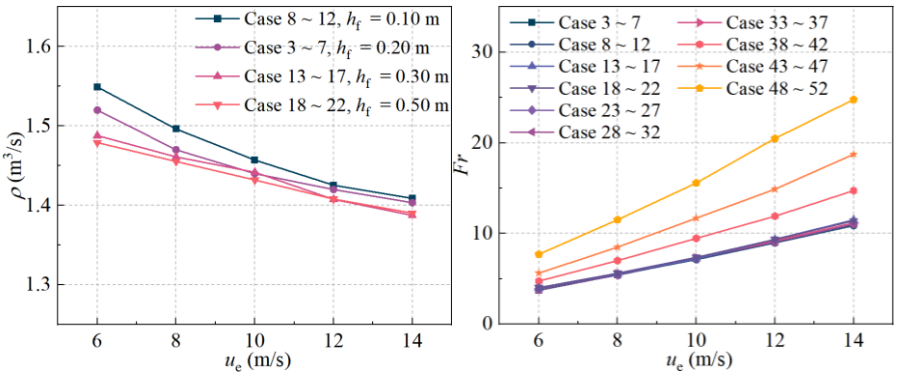

(c) *(d)*

Figure 9. *Variation of ρ and Fr (a) w/h; (b) vent area; (c) h_f; (d) Fr.*

3.3. Exhaust efficiency

Exhaust efficiency is another critical index for evaluating the performance of ventilation systems in heavy gas elimination scenarios. As defined by (Vauquelin, 2008), exhaust efficiency is quantified as the ratio of two key parameters: the total mass flow rate of heavy gas discharged through the vents and the total mass flow rate of heavy gas present in the tunnel under natural conditions (i.e., without mechanical exhaust). This efficiency metric directly reflects the capability of the ventilation system to capture and remove heavy gas, making it a reliable quantitative indicator for assessing the overall performance of heavy gas elimination systems. The specific mathematical definition of exhaust efficiency is as follows:

$$\varepsilon = \frac{M_e}{M} \tag{8}$$

where M is the mass flow flux of heavy gas in the tunnel without mechanical exhaust:

$$M = W\int_0^{h_t} \rho u dz \tag{9}$$

where W is the width of the tunnel, m.

This section compares the effects of w/h, A, and h_f on exhaust efficiency, with the results presented in Figure 10. As shown in the figure, under the same exhaust volume, the vents achieve the optimal exhaust performance when the w/h is 1.53. At a fixed u_e, exhaust efficiency decreases with an increase in A. For instance: When A is 2 m^2 , the exhaust efficiency values at u_e of 6 m/s and 14 m/s are 0.18 and 0.09, respectively—representing a decrease of 47.9%. When A is 1 m^2 , the exhaust efficiency values at u_e = 6 m/s and u_e = 14 m/s are 0.11 and 0.09, respectively—corresponding to a decrease of 17.3%. These results indicate that for a given A, there exists an optimal u_e that maximizes exhaust efficiency. Additionally, exhaust efficiency increases as h_f decreases, and this trend is particularly pronounced at high u_e. Specifically, when u_e = 14 m/s, the exhaust efficiency at h_f = 0.1 m is 14.4% higher than that at h_f = 0.5 m.

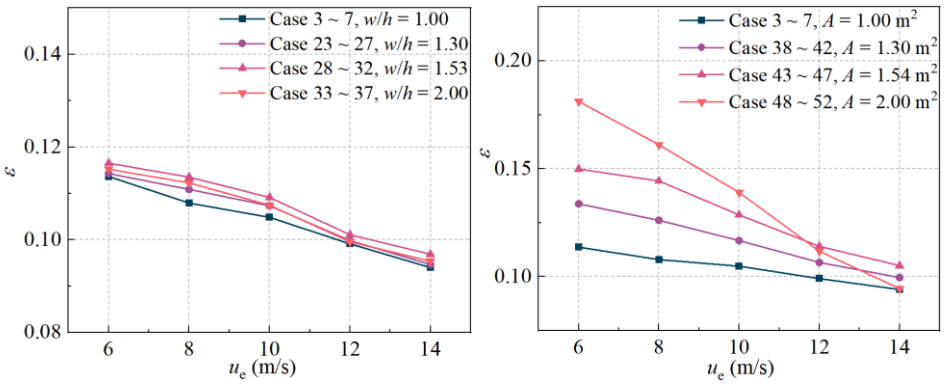

(a) *(b)*

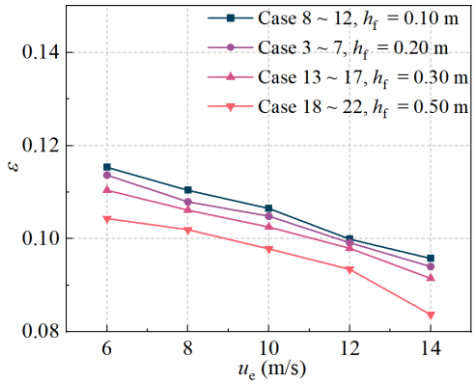

(c)

Figure 10. *Variation of* ε *under different (a) w/h; (b) vent area; (c)* h_f.

4. CONCLUSION

This study investigated the effects of three key parameters—vent aspect ratio *w*/*h*, vent area *A*, and vent height above the ground h_f — on the performance of side-mounted exhaust vents for addressing heavy gas leakage in tunnels. Vent performance was evaluated from three dimensions: the height of the heavy gas layer downstream of the vents, the exhaust Froude number *Fr* and exhaust efficiency ε. The main conclusions are as follows:

(1) Increasing the *w*/*h* and *A* can reduce the height of the heavy gas layer downstream of the vents. Within the parameter range of this study, there exists an optimal vent height h_f of 0.1 m; under the same exhaust volume, this height results in the lowest heavy gas height downstream the vent.

(2) The average heavy gas density at the vent inlet is inversely proportional to both *A* and h_f. Excessively large *A* or h_f can lead to the entrainment and discharge of fresh air through the vents, even at low u_e. This fresh air entrainment dilutes the heavy gas concentration at the vent inlet, which is detrimental to efficient heavy gas elimination.

(3) At relatively low u_e, increasing *A* can improve ε; however, at high u_e, increasing *A* significantly reduces ε. Within the scope of this study, the maximum ε was achieved when the vent area was 2 m² and the exhaust velocity was 6 m/s.

It is important to note that when designing ventilation systems for heavy gas elimination, ε must be considered in conjunction with the heavy gas mass flow rate discharged through the vents. The core design objective is to maximize the heavy gas mass flow rate while minimizing fresh air entrainment and discharge. Future research will focus on two directions: first, conducting experimental validation of the heavy gas elimination performance simulated in this study; second, explore the design methodology of a ventilation system that balances smoke extraction and heavy gas elimination, aiming to achieve optimal hazard prevention effects.

ACKNOWLEDGMENTS

The study was supported by Shaanxi Province Technical Innovation Guidance Special Project (No. 2023GXLH-051), Foundation of International Joint Laboratory on Low Carbon Built Environment, Ministry of Education (Xi'an University of Architecture and Technology). The authors are grateful for the support.

REFERENCES

[1] Blackmore, D.R., Herman, M.N., Woodward, J.L., 1982. Heavy gas dispersion models. Journal of Hazardous Materials 6, 107-128.doi:https://doi.org/10.1016/0304-3894(82)80036-8

[2] Cai, J., Chen, J., Ahmad, S., Zhao, J., Cheng, H., Zi, S., Xiao, J., 2020. Investigation into the effect of upstream obstacles and hazardous sources on dispersion in the urban environment with LES model. Journal of Hazardous Materials 390, 121953.doi:https://doi.org/10.1016/j.jhazmat.2019.121953

[3] Cong, H., Bi, M., Bi, Y., Li, Y., Jiang, H., Gao, W., 2021. Experimental studies on the smoke extraction performance by different types of ventilation shafts in extra-long road tunnel fires. Tunnelling and Underground Space Technology 115, 104029.doi:https://doi.org/10.1016/j.tust.2021.104029

[4] Fatahian, E., Salarian, H., Fatahian, H., 2020. Numerical Investigation of Hazardous Gas Dispersion Over Obstacles and Residential Areas. International Journal of Engineering 33, 2087-2094.doi:https://doi.org/10.5829/ije.2020.33.10a.27
[5] Gao, N., Wang, R., Wu, Y., Wu, Z., 2023. Study on impact factors of tracer gas method in investigations of gaseous pollutant transport and building ventilation. Building Simulation 16, 413-426.doi:https://doi.org/10.1007/s12273-022-0947-3
[6] Han, O., Zhang, Y., Li, A., Li, J., Li, Y., Liu, H., 2020. Experimental and numerical study on heavy gas contaminant dispersion and ventilation design for industrial buildings. Sustainable Cities and Society 55, 102016.doi:https://doi.org/10.1016/j.scs.2020.102016
[7] Hanna, S.R., Chang, J.C., Strimaitis, D.G., 1993. Hazardous gas model evaluation with field observations. Atmospheric Environment. Part A. General Topics 27, 2265-2285.doi:https://doi.org/10.1016/0960-1686(93)90397-H
[8] Hou, J., Gai, W.-m., Cheng, W.-y., Deng, Y.-f., 2021. Hazardous chemical leakage accidents and emergency evacuation response from 2009 to 2018 in China: A review. Safety Science 135, 105101.doi:https://doi.org/10.1016/j.ssci.2020.105101
[9] Inc, A., 2022. ANSYS Fluent Theory Guide.
[10] Kassomenos, P., Karayannis, A., Panagopoulos, I., Karakitsios, S., Petrakis, M., 2008. Modelling the dispersion of a toxic substance at a workplace. Environmental Modelling & Software 23, 82-89.doi:https://doi.org/10.1016/j.envsoft.2007.05.003
[11] Lei, P., Chen, C., Jiao, W., Shi, C., 2023. Experimental study on collaborative longitudinal ventilation of smoke control for branched tunnel fires considering different branch angles. Tunnelling and Underground Space Technology 136, 105097.doi:https://doi.org/10.1016/j.tust.2023.105097
[12] Li, G., Wang, J., Wang, M., Lin, Y., Yu, X., Zong, R., 2023a. Experimental and numerical study of heavy gas dispersion in presence of obstacle motion. Process Safety and Environmental Protection 177, 1494-1505.doi:https://doi.org/10.1016/j.psep.2023.07.092
[13] Li, Y., Yang, J., Wu, X., Zhou, P., Liu, Y., Han, X., 2023b. Explosion risk analysis of R290 leakage into a limited external space. Applied Thermal Engineering 225, 120122.doi:https://doi.org/10.1016/j.applthermaleng.2023.120122
[14] Ma, Y., Li, A., Che, J., Wang, T., Yang, C., Che, L., Liu, J., 2023. Investigation of heavy gas dispersion characteristics in a static environment: Spatial distribution and volume flux prediction. Building and Environment 242, 110501.doi:https://doi.org/10.1016/j.buildenv.2023.110501
[15] Ma, Y., Li, A., Wang, T., Che, J., Yang, C., Zhang, X., Wu, D., 2025. Characteristics of inclined negatively buoyant jet of dense gas leakage. Physics of Fluids 37, 025123.doi:https://doi.org/10.1063/5.0251179
[16] Vauquelin, O., 2008. Experimental simulations of fire-induced smoke control in tunnels using an "air–helium reduced scale model": Principle, limitations, results and future. Tunnelling and Underground Space Technology 23, 171-178.doi:https://doi.org/10.1016/j.tust.2007.04.003
[17] Wang, T., Li, A., Ma, Y., Zhang, Y., 2025. Analysis of parameters for top exhaust ventilation to minimize heavy gas dispersion in fixed leakage source spaces. Journal of Building Engineering 103, 112091.doi:https://doi.org/10.1016/j.jobe.2025.112091
[18] Wang, T., Li, A., Ma, Y., Zhang, Y., Yin, H., 2024. Enhancing heavy gas capture in confined spaces through ventilation control technology. Building Simulation 17, 1161-1182.doi:10.1007/s12273-024-1131-8
[19] Wang, Z., Hu, Y., Jiang, J., 2013. Numerical investigation of leaking and dispersion of carbon dioxide indoor under ventilation condition. Energy and Buildings 66, 461-466.doi:https://doi.org/10.1016/j.enbuild.2013.06.031
[20] Xing, J., Liu, Z., Huang, P., Feng, C., Zhou, Y., Zhang, D., Wang, F., 2013. Experimental and numerical study of the dispersion of carbon dioxide plume. Journal of Hazardous Materials 257, 40-48.doi:https://doi.org/10.1016/j.jhazmat.2013.03.066
[21] Zeng, L., Gao, J., Lv, L., Du, B., Zhang, Y., Zhang, R., Ye, W., Zhang, X., 2021. Localization and characterization of intermittent pollutant source in buildings with ventilation systems: Development and validation of an inverse model. Building Simulation 14, 841-855.doi:https://doi.org/10.1007/s12273-020-0706-2
[22] Zhang, Y., Wang, L., Li, A., Tao, P., 2020. Performance evaluation by computational fluid dynamics modelling of the heavy gas dispersion with a low Froude number in a built environment. Indoor Built Environment 29, 656-670.doi:https://doi.org/https://doi.org/10.1177/1420326X19856041